NASA TECHNICAL NOTE

NASA TN D-5898

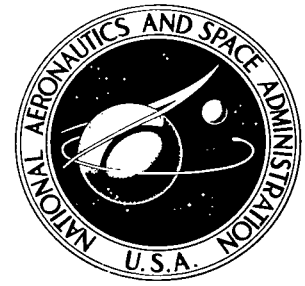

AERODYNAMIC INTERFERENCE EFFECTS ON HALF-CONE BODIES WITH THIN WINGS AT MACH 10.03

by James C. Townsend

Langley Research Center
Hampton, Va. 23365

NATIONAL AERONAUTICS AND SPACE ADMINISTRATION • WASHINGTON, D. C. • JULY 1970

1. Report No.	2. Government Accession No.	3. Recipient's Catalog No.
NASA TN D-5898		

4. Title and Subtitle

AERODYNAMIC INTERFERENCE EFFECTS ON HALF-CONE BODIES WITH THIN WINGS AT MACH 10.03

5. Report Date: July 1970

6. Performing Organization Code:

7. Author(s)

James C. Townsend

8. Performing Organization Report No.: L-6487

9. Performing Organization Name and Address

NASA Langley Research Center
Hampton, Va. 23365

10. Work Unit No.: 722-01-10-07

11. Contract or Grant No.:

12. Sponsoring Agency Name and Address

National Aeronautics and Space Administration
Washington, D.C. 20546

13. Type of Report and Period Covered: Technical Note

14. Sponsoring Agency Code:

15. Supplementary Notes

16. Abstract

Halves of cone bodies having fineness ratios of 2, 4, or 6 were tested with thin flat wings at Mach 10.03 and Reynolds numbers of 1.2×10^6, 1.5×10^6, or 1.8×10^6. Several wing planforms designed empirically or theoretically to match the shape of the shock wave about the body were investigated for each fineness ratio. Tests were also made with thick wings and with wings having various leading-edge shapes. The wing planforms which matched the actual shock shape provide the highest lift-drag ratios. Increasing the fineness ratio of the half-cone body increases the lift-drag ratio but decreases the lift coefficient. Effects of wing thickness and leading-edge shape were very small.

17. Key Words (Suggested by Author(s))

Hypersonic flow
Aerodynamic interference
Half-cone bodies

18. Distribution Statement

Unclassified – Unlimited

19. Security Classif. (of this report)	20. Security Classif. (of this page)	21. No. of Pages	22. Price*
Unclassified	Unclassified	24	$3.00

*For sale by the Clearinghouse for Federal Scientific and Technical Information
Springfield, Virginia 22151

AERODYNAMIC INTERFERENCE EFFECTS ON HALF-CONE BODIES WITH THIN WINGS AT MACH 10.03

By James C. Townsend
Langley Research Center

SUMMARY

Halves of cone bodies having fineness ratios of 2, 4, or 6 were tested with thin flat wings at Mach 10.03 and Reynolds numbers of 1.2×10^6, 1.5×10^6, or 1.8×10^6. Several wing planforms designed empirically or theoretically to match the shape of the shock wave about the body were investigated for each fineness ratio. Tests were also made with thick wings and with wings having various leading-edge shapes. The theoretical shock-wave-shape estimates used are inadequate for the fineness-ratio-4 and 6 cones. The wing planforms which matched the actual shock shape provide the highest lift-drag ratios. Increasing the fineness ratio of the half-cone body increases the lift-drag ratio but decreases the lift coefficient. Effects of wing thickness and leading-edge shape were very small.

INTRODUCTION

A number of hypersonic vehicle applications require high lift-drag ratios. Favorable aerodynamic interference can contribute toward achieving this requirement. Thus, the National Aeronautics and Space Administration has been studying configurations for which useful interference may occur. One such configuration is a body mounted beneath a thin flat wing (e.g., refs. 1, 2, and 3). According to inviscid theory, the wing acts as a reflection plane for the body, maintaining the flow field that would occur for the corresponding symmetric configuration. In turn, the body pressure field inside the bow shock wave adds to the normal force on the wing. These interference pressures around the body and on the wing should contribute to the aerodynamic efficiency of the combination. Because of the relatively large skin-friction drag at hypersonic speeds, any part of the wing outside the body shock would be inefficient as a lifting surface at small angles of attack. Thus, wing planforms which match the shock-wave shape about the body should give the greatest interference benefits.

The purpose of the present experimental study was to determine the aerodynamic characteristics of wing—half-cone-body configurations with the wings designed from interference principles – that is, the leading edges of the thin wings were to coincide

with the cone shock wave at the design Mach number. However, several analytical methods produced varying predictions of the shock-wave shape depending on the order of terms retained and whether boundary-layer displacement effects were included. Tests of models designed according to the various predictions allow an evaluation of the accuracy of the methods used and of the sensitivity of the useful interference to deviations from the ideal planform.

The tests were made in air in the Langley 15-inch hypersonic flow apparatus at Mach number 10.03. The Reynolds number at the nominal test conditions was 1.2×10^6, 1.5×10^6, or 1.8×10^6 depending on model length. Each body was a half of a fineness-ratio-2, 4, or 6 right circular cone. In addition to tests with the several planforms of thin wings, the bodies were tested without wings and with thick wings having various leading-edge shapes. The nominal angle-of-attack range was from -8° to $+8^\circ$.

SYMBOLS

$\bar{c}$	mean aerodynamic chord
C	Chapman-Rubesin constant, $\frac{\mu}{T}\frac{T_r}{\mu_r}$
C_D	drag coefficient, $\frac{D}{qS}$
C_L	lift coefficient, $\frac{L}{qS}$
C_m	pitching-moment coefficient, $\frac{\text{Pitching moment}}{qS\bar{c}}$
D	drag
f	twice the cone fineness ratio, $\left(l/r_b\right)_B$
l	body length
L	lift
m	power-law exponent
M	free-stream Mach number
p_t	tunnel stagnation pressure

q	dynamic pressure
r	radial cylindrical coordinate
R	shock-wave radius and wing radial coordinate
R_l	Reynolds number based on free-stream conditions and body length
S	planform area
t	wing thickness
T	temperature
T_t	tunnel stagnation temperature
x	axial coordinate
α	angle of attack, referenced to axis of symmetry of full cone
γ	ratio of specific heats
δ	shock-wave shape parameter, $(R_0/l)_B$
δ^*	boundary-layer displacement thickness
η	normalized radial coordinate, r/R_0
θ	conical half-angle
μ	viscosity coefficient
σ	Mach number perturbation parameter

Subscripts:

b	body
B	base of body

c	cone
E	exact cone theory
max	maximum
r	reference
s	shock wave
w	wing
0	zeroth-order theory
1	first-order theory

Primed quantities include effects of boundary-layer displacement thickness.

THEORETICAL CONSIDERATIONS

Several theoretical estimates of the shock-wave shapes were made in order to design the matching wing planforms. If the conical bodies are considered to be power-law bodies of revolution (with the power-law exponent equal to 1), a form of hypersonic similarity solution applies.* With the shock-wave radius given by $\frac{R_0}{\delta l} = \left(\frac{x}{l}\right)^m$, the flow is similar along curves $\frac{r}{\delta l} = \eta\left(\frac{x}{l}\right)^m$. (See sketch 1.) In particular, the body radius is $\frac{r_b}{\delta l} = \eta_b\left(\frac{x}{l}\right)^m$ where the value of η_b for each m is found by solving the flow equations (ref. 4). In terms of the body radius, the shock radius is then

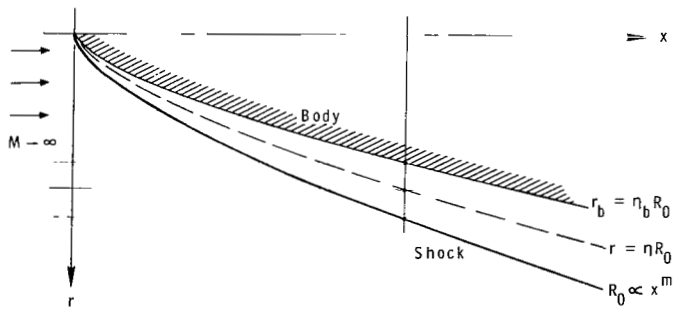

Sketch 1

$$R_0 = \frac{r_b}{\eta_b} \tag{1}$$

This shock radius is a "zero-order" estimate in that it applies as $M \to \infty$.

*This solution was used in anticipation of future work utilizing power-law bodies.

To obtain the effect of finite Mach numbers to first order, a perturbation is applied so that

$$R_1 = \frac{r_b}{\eta_b}(1 + \sigma) \tag{2}$$

According to reference 4, the shock-wave angle is related to the cone angle by $\frac{\theta_s}{\theta_c} = 1.092\left(1 + \frac{0.332}{M^2\theta_c^2}\right)$ for $\theta_c << 1$. (Note that these angles are measured in radians.) Hence,

$$1 + \sigma = \eta_b \frac{R_1}{r_b} = \eta_b \frac{\tan \theta_s}{\tan \theta_c} = f\eta_b \tan\left[1.092\theta_c\left(1 + \frac{0.332}{M^2\theta_c^2}\right)\right]$$

$\left(\text{note that } \tan \theta_c = 1/f\right)$.

The shock-wave angle θ_s can also be found from exact numerical solutions for inviscid flow over cones. Then,

$$R_E = x \tan \theta_s = r_b f \tan \theta_s \tag{3}$$

where θ_s is here found from tables such as those of reference 5.

The foregoing estimates do not account for the outward displacement of the shock wave caused by growth of the boundary layer (B.L.) To include this effect, the boundary-layer displacement thickness δ^* was added to the body radius to obtain an effective radius $r_b' = r_b + \delta^*$. Replacing r_b with $r_b + \delta^*$ in equations (1), (2), and (3) produced the following estimates of shock-wave radius:

$$R_0' = \frac{1}{\eta_b}\left(r_b + \delta^*\right) \tag{4}$$

$$R_1' = \frac{\left(r_b + \delta^*\right)}{\eta_b}(1 + \sigma) \tag{5}$$

$$R_E' = \left(r_b + \delta^*\right) f \tan \theta_s \tag{6}$$

The same values of η_b, σ, and θ_w were used as in the equations without boundary-layer effects. The displacement thickness was calculated by the following equation for adiabatic, laminar boundary layers from reference 4, evaluated for $m = 1$:

$$\frac{\delta^*}{l} = 0.736\eta_b f M(\gamma - 1)\sqrt{\frac{C}{\gamma R_l}}\left(\frac{x}{l}\right)^{1/2} \tag{7}$$

The Chapman-Rubesin constant C was taken to be 1.0. For m = 1, reference 6 gives $\eta_b = 0.915$. Note that for large-scale vehicles, regions of the boundary layer may become turbulent; therefore, an appropriate method (e.g., refs. 7 and 8) is required for calculation of the displacement thickness.

MODELS

Three full cones were made so that actual shock-wave shapes could be measured from schlieren photographs. These right, circular, stainless-steel cones with fineness ratios of 2, 4, and 6 were 8.00, 10.00, and 12.00 inches (20.32, 25.40, and 30.48 cm) in length, respectively. The bodies for the interference tests were longitudinal halves of identical cones and thus had effective fineness ratios of $2\sqrt{2}$, $4\sqrt{2}$, and $6\sqrt{2}$. The wings were 0.020-inch-thick (0.051 cm) stainless-steel sheets brazed to the bodies. (Thinner wings were not practical for fabrication.) Figure 1(a) shows a representative wing-body model. Model designations and dimensions are given in table I. Ordinates of the wings with curved leading edges are presented in table II. Models $W_0 2$, $W_0 4$, and $W_0 6$ had wings with straight leading edges which matched the shock-wave shapes about the three fineness-ratio cones as given by the zero-order theory (eq. (1)). First-order theory (eq. (2)) gave models $W_1 2$, $W_1 4$, and $W_1 6$ which also had wings with straight leading edges. By adding the boundary-layer correction to the zero-order theory (eq. (4)), models $W_0' 2$, $W_0' 4$, and $W_0' 6$ were obtained; by adding the correction to the first-order theory (eq. (5)), models $W_1' 2$, $W_1' 4$, and $W_1' 6$ were obtained. Exact theory for the fineness-ratio-2 cone gave model $W_E 2$ (without boundary-layer correction, eq. (3)) and model $W_E' 2$ (with boundary-layer correction, eq. (6)). Planforms for models $W_M 2$ and $W_M 6$ were smoothed shock-wave shapes from schlieren photographs of the flow about the fineness-ratio-2 and 6 cones.

A variant of model $W_E' 2$ with the leading edge sharpened was designated model $W_E' 2S$. Additional models with the same planforms as $W_E' 2$, $W_1' 4$, and $W_1' 6$ but with wings 0.090 inch (0.229 cm) thick were designated $W_E' 2S$, $W_E' 2T$, $W_1' 4T$, $W_1' 4S$, $W_1' 4A$, $W_1' 4B$, and $W_1' 6T$. Figure 1(b) shows the leading-edge shapes for these wings. Photographs of representative models are presented as figure 2.

Thermal stresses due to the high recovery temperatures deformed the wings of models $W_1' 4$ and $W_1' 6$ into a permanent waviness which may be seen in figure 2(c). The maximum amplitude was two wing thicknesses with a wavelength approximately twice the wing overhang. This amount of distortion is believed to have had no significant effect on the test results.

TESTS

The Langley 15-inch hypersonic flow apparatus used for the tests is a blow-down-type facility which has a running time of $2\frac{1}{2}$ minutes and provides an average test-section Mach number of 10.03 in air. This facility is described more completely in reference 9. For the present tests, the nominal stagnation conditions were $p_t = 972$ psia (6700 kN/m^2) and $T_t = 1106^\circ$ F (870° K), which give a test-section Reynolds number of 1.5×10^5 per inch (5.91×10^6 per m). The Reynolds numbers based on length of the bodies with cone fineness ratios of 2, 4, and 6 were thus 1.2×10^6, 1.5×10^6, and 1.8×10^6. Thus, the boundary layers on all models were probably completely laminar. Although the static pressure and temperature reached the range for air liquefaction under equilibrium conditions, references 10 and 11 along with a corroborating test in this study (fig. 3) have shown that there is sufficient supersaturation under the present test conditions to avoid condensation effects.

A six-component, strain-gage balance in the model measured the forces and moments. A heat-conduction type of absolute pressure gage mounted in the sting measured the base pressure. By assuming that this pressure is constant over the entire model base, the axial-force coefficient was adjusted to the condition of free-stream static pressure on the base. This correction varied approximately from -0.0034 for cone fineness ratio 2 down to -0.0005 for cone fineness ratio 6. The angle of attack was varied from approximately -8° to 8° and was referenced to the cone axis of symmetry. Tests of some models were repeated as indicated by multiple points in the data figures.

RESULTS AND DISCUSSION

Shock-Wave Shapes

In figure 3, the shock-wave shapes for the full-cone models are compared with the predicted shapes obtained from equations (1) to (6). For the fineness-ratio-2 cone, the shock shapes obtained by means of the exact and first-order theories with boundary-layer displacement thickness included agree well with the experimentally measured shock location. When the cone angle is smaller, the shock wave is closer to the body than these theories predict. Adiabatic wall conditions are assumed in the estimation of boundary-layer displacement thickness by equation (7). Inasmuch as the actual surface temperature of the cone was on the order of one-half the adiabatic recovery temperature, the actual displacement thickness was somewhat less and the actual shock location was nearer the body than estimated. This effect is less important for larger cone angles since the boundary layer is then thinner. Note that the theoretical shock-wave shapes of figure 3 are approximately the wing shapes of the models.

Wing-Planform Variation

The principal aerodynamic characteristics for the several wing planforms of the three fineness-ratio models are presented in figure 4. The wings have a relatively small effect on the aerodynamic characteristics inasmuch as there are no large deviations from the data for the half-cone bodies alone (circles). In particular, the lift coefficients at zero angle of attack are little affected; there is a small loss which is partially recouped as wing area is increased. Since $\alpha = 0^{o}$ is the design condition for the wings, this point must be examined more closely. The flat-plate wing alone produces no lift at zero angle of attack; therefore, in this particular case a lift coefficient based on some constant area provides a better comparison of the effects of wing planform. In figure 5, the lift coefficient at $\alpha = 0^{o}$ based on the body planform area is plotted against the normalized exposed wing area. Here, $S_s - S_b$ is the exposed area of a wing whose planform matches the empirical shock-wave shape. Note that since both the planform shapes and areas varied, these sets of points do not form smooth curves and thus the fairings only indicate the data trend. The lift generally increases from a low point for very small wings as the wing approaches the empirical shock-wave shape $\left(\frac{S_w - S_b}{S_s - S_b} = 1\right)$. As expected, the data show no further increase for larger wing areas. The lift-drag ratio at $\alpha = 0^{o}$ follows the same trend as the lift (fig. 5), but the increase with wing area is smaller since the drag rises with the increased wetted area. For the wing with considerable area outside the body shock wave, $(L/D)_{\alpha=0^{o}}$ drops as the drag continues to rise with no increase in lift. The same trend occurs for $(L/D)_{max}$ although the levels are different. As can be seen from figure 4, the angles of attack at $(L/D)_{max}$ are low; therefore, the wing area outside the body shock wave does not provide much lift. These observations bear out the expectation that the wing planforms should match the shape of the shock wave about the body. However, this design condition is not critical in that L/D and C_L are little changed by moderately large variations in exposed wing area.

Body-Fineness-Ratio Variation

The aerodynamic characteristics for the three body fineness ratios are compared in figure 6. The planforms of the three wings in figure 6(a) are those nearest matching the shock-wave shape about the body. The characteristics of the three bodies with no wings are shown in figure 6(b). For cone fineness ratio 2, the lift-drag ratio at the design condition ($\alpha = 0^{o}$) is very near the maximum lift-drag ratio. As the fineness ratio increases, the angle of attack for $(L/D)_{max}$ also increases and the L/D curve becomes more peaked. Thus, $(L/D)_{\alpha=0^{o}}$ is highest for a cone fineness ratio near 4, whereas $(L/D)_{max}$ continues to increase with fineness ratio. Since the available lift coefficient decreases at the same time, the choice of an optimum fineness ratio depends on a trade-off between C_L and L/D.

With increasing fineness ratio, the variation with angle of attack of the pitching moment about the chosen moment reference center changes from slightly stable to slightly unstable. However, with a reasonable center-of-gravity location the configurations could be made stable in pitch throughout the test angle-of-attack range.

Wing Thickness and Leading-Edge Shape

The aerodynamic characteristics for two wing thicknesses and several leading-edge shapes are presented in figure 7. The fairings in this figure are through the data for the thin-wing models $\left(W'_E2, W'_14, W'_16\right)$. For all three fineness ratios, the effects of wing thickness and leading-edge shape are small. The thicker wing causes a 10-percent higher drag than the thin wing at low lift for cone fineness ratio 2. For the more highly swept wing of the cone-fineness-ratio-6 configuration, the effect of wing thickness was negligible. Similarly, the different wing-leading-edge shapes (fig. 7(b)) do not have any significant effect on the aerodynamic characteristics of the cone-fineness-ratio-4 configuration. Thus, aerodynamic heating may determine the wing-leading-edge shape for this type of configuration with little penalty in aerodynamic performance.

CONCLUSIONS

An investigation of half-cone bodies with thin flat wings was conducted at a Mach number of 10.03. The nominal Reynolds numbers for models with cone fineness ratios of 2, 4, and 6 were 1.2×10^6, 1.5×10^6, and 1.8×10^6, respectively. Several wing planforms, designed empirically and theoretically with varying degrees of accuracy to match the shock shape about the body, were tested for each fineness ratio. In addition, tests were made with thick wings and with wings having various leading-edge shapes. The test results lead to the following conclusions:

1. The theoretical methods used to find the shapes of shock waves about a body are not adequate for cone fineness ratios greater than 2 at Mach 10. At higher fineness ratios it is necessary to have a better estimate for the boundary-layer displacement thickness.

2. The most effective wing planforms in terms of lift-drag ratio are those which approximately match the shock wave about the full body at zero angle of attack.

3. Increasing the cone fineness ratio under the given test conditions increases the maximum lift-drag ratio but decreases the available lift coefficient.

4. The effects of wing thickness and leading-edge shape are relatively small. Thus, aerodynamic heating may determine these geometrical parameters.

Langley Research Center,
National Aeronautics and Space Administration,
Hampton, Va., May 6, 1970.

REFERENCES

1. Eggers, A. J., Jr.; and Syvertson, Clarence A.: Aircraft Configurations Developing High Lift-Drag Ratios at High Supersonic Speeds. NACA RM A55L05, 1956.

2. Johnston, Patrick J.; Snyder, Curtis D.; and Witcofski, Robert D.: Maximum Lift-Drag Ratios of Delta-Wing—Half-Cone Combinations at a Mach Number of 20 in Helium. NASA TN D-2762, 1965.

3. Fetterman, David E.: Favorable Interference Effects on Maximum Lift-Drag Ratios of Half-Cone Delta-Wing Configurations at Mach 6.86. NASA TN D-2942, 1965.

4. Kubota, Toshi: Inviscid Hypersonic Flow Over Blunt-Nosed Slender Bodies. 1957 Heat Transfer and Fluid Mechanics Institute, Stanford Univ. Press, June 1957, pp. 193-210.

5. Sims, Joseph L.: Tables for Supersonic Flow Around Right Circular Cones at Zero Angle of Attack. NASA SP-3004, 1964.

6. Mirels, Harold: Approximate Analytical Solutions for Hypersonic Flow Over Slender Power Law Bodies. NASA TR R-15, 1959.

7. Spalding, D. B.; and Chi, S. W.: The Drag of a Compressible Turbulent Boundary Layer on a Smooth Flat Plate With and Without Heat Transfer. J. Fluid Mech., vol. 18, pt. 1, Jan. 1964, pp. 117-143.

8. Persh, Jerome; and Lee, Roland: Tabulation of Compressible Turbulent Boundary Layer Parameters. NAVORD Rep. 4282, May 1, 1956.

9. Putnam, Lawrence E.; and Brooks, Cuyler W., Jr.: Static Longitudinal Aerodynamic Characteristics at a Mach Number of 10.03 of Low-Aspect-Ratio Wing-Body Configurations Suitable for Reentry. NASA TM X-733, 1962.

10. Daum, Fred L.: Air Condensation in a Hypersonic Wind Tunnel. AIAA J., vol. 1, no. 5, May 1963, pp. 1043-1046.

11. Putnam, Lawrence E.: Investigation of Effects of Ramp Span and Deflection Angle on Laminar Boundary-Layer Separation at Mach 10.03. NASA TN D-2833, 1965.

TABLE I.- MODEL DESIGNATIONS AND GEOMETRIC CHARACTERISTICS

Model*	Fineness ratio of cone	Length, l		Planform area ratio, S/S_b	Ratio of mean aerodynamic chord to body length, $\bar{c}/l$	Ratio of wing radial coordinate to body length, R_B/l	Remarks
		in.	cm				
B2	2	8.00	20.32	1.0000	0.6667	0.2500	Half-cone body alone, no wing.
B4	4	10.00	25.40	1.0000	.6667	.1250	
B6	6	12.00	30.48	1.0000	.6667	.0833	
$W_0$2	2	8.00	20.32	1.0940	0.6667	0.2735	Zero-order theory without boundary layer (eq. (1)).
$W_0$4	4	10.00	25.40	1.0953	.6667	.1369	
$W_0$6	6	12.00	30.48	1.0940	.6667	.0912	
$W_1$2	2	8.00	20.32	1.1601	0.6667	0.2900	First-order theory without boundary layer (eq. (2)).
$W_1$4	4	10.00	25.40	1.3312	.6667	.1664	
$W_1$6	6	12.00	30.48	1.6220	.6667	.1352	
W_E2	2	8.00	20.32	1.1848	0.6667	0.2963	Exact cone theory without boundary layer (eq. (3)).
$W'_0$2	2	8.00	20.32	1.1418	0.6718	0.2825	Zero-order theory with boundary-layer correction (eq. (4)).
$W'_0$4	4	10.00	25.40	1.2616	.6838	.1525	
$W'_0$6	6	12.00	30.48	1.4368	.6977	.1127	
$W'_1$2	2	8.00	20.32	1.2066	0.6717	0.2988	First-order theory with boundary-layer correction (eq. (5)).
$W'_1$4, $W'_1$4T, $W'_1$4S, $W'_1$4A, $W'_1$4B	4	10.00	25.40	1.4966	.6811	.1819	
$W'_1$6, $W'_1$6T	6	12.00	30.48	1.9975	.7418	.1665	
W'_E2, W'_E2S, W'_E2T	2	8.00	20.32	1.2313	0.6716	0.3049	Exact cone theory with boundary-layer correction (eq. (6)).
W_M2	2	8.00	20.32	1.2253	0.6768	0.3011	Empirical (from measured shock-wave shapes).
W_M6	6	12.00	30.48	1.7411	.6812	.1408	

*Model notation:

B body alone

W wing-body combination

Suffixes A, B, S, and T denote leading-edge shapes shown in figure 1.

TABLE II.- ORDINATES OF WINGS WITH CURVED LEADING EDGES

x/l	R/l								
	$W_0'2$	$W_1'2$	$W_E'2$, $W_E'2S$, $W_E'2T$	W_M2	$W_0'4$	$W_1'4$, $W_1'4T$, $W_1'4S$, $W_1'4A$, $W_1'4B$	$W_0'6$	$W_1'6$, $W_1'6T$	W_M6
0.05	0.0156	0.0165	0.0168	0.0182	0.0103	0.0118	0.0093	0.0138	0.0088
.10	.0301	.0318	.0324	.0347	.0186	.0216	.0159	.0235	.0164
.15	.0445	.0469	.0478	.0505	.0266	.0310	.0220	.0325	.0237
.20	.0587	.0619	.0631	.0654	.0344	.0402	.0278	.0411	.0311
.25	.0728	.0769	.0784	.0806	.0420	.0494	.0335	.0495	.0382
.30	.0869	.0918	.0936	.0949	.0496	.0584	.0391	.0578	.0451
.35	.1010	.1067	.1088	.1090	.0571	.0674	.0446	.0659	.0521
.40	.1150	.1215	.1240	.1228	.0646	.0764	.0500	.0739	.0592
.45	.1291	.1364	.1391	.1376	.0721	.0853	.0554	.0819	.0660
.50	.1431	.1512	.1543	.1527	.0795	.0942	.0607	.0898	.0731
.55	.1571	.1660	.1694	.1677	.0869	.1030	.0660	.0976	.0802
.60	.1705	.1808	.1845	.1826	.0942	.1119	.0713	.1054	.0874
.65	.1850	.1956	.1996	.1976	.1016	.1207	.0765	.1131	.0941
.70	.1990	.2103	.2146	.2125	.1089	.1295	.0818	.1208	.1007
.75	.2129	.2251	.2297	.2277	.1162	.1382	.0869	.1285	.1077
.80	.2269	.2398	.2448	.2424	.1235	.1470	.0921	.1362	.1142
.85	.2408	.2546	.2598	.2571	.1308	.1557	.0973	.1438	.1208
.90	.2547	.2693	.2749	.2719	.1380	.1644	.1024	.1514	.1275
.95	.2686	.2840	.2899	.2868	.1453	.1732	.1075	.1589	.1341
1.00	.2825	.2988	.3049	.3011	.1525	.1819	.1127	.1665	.1408

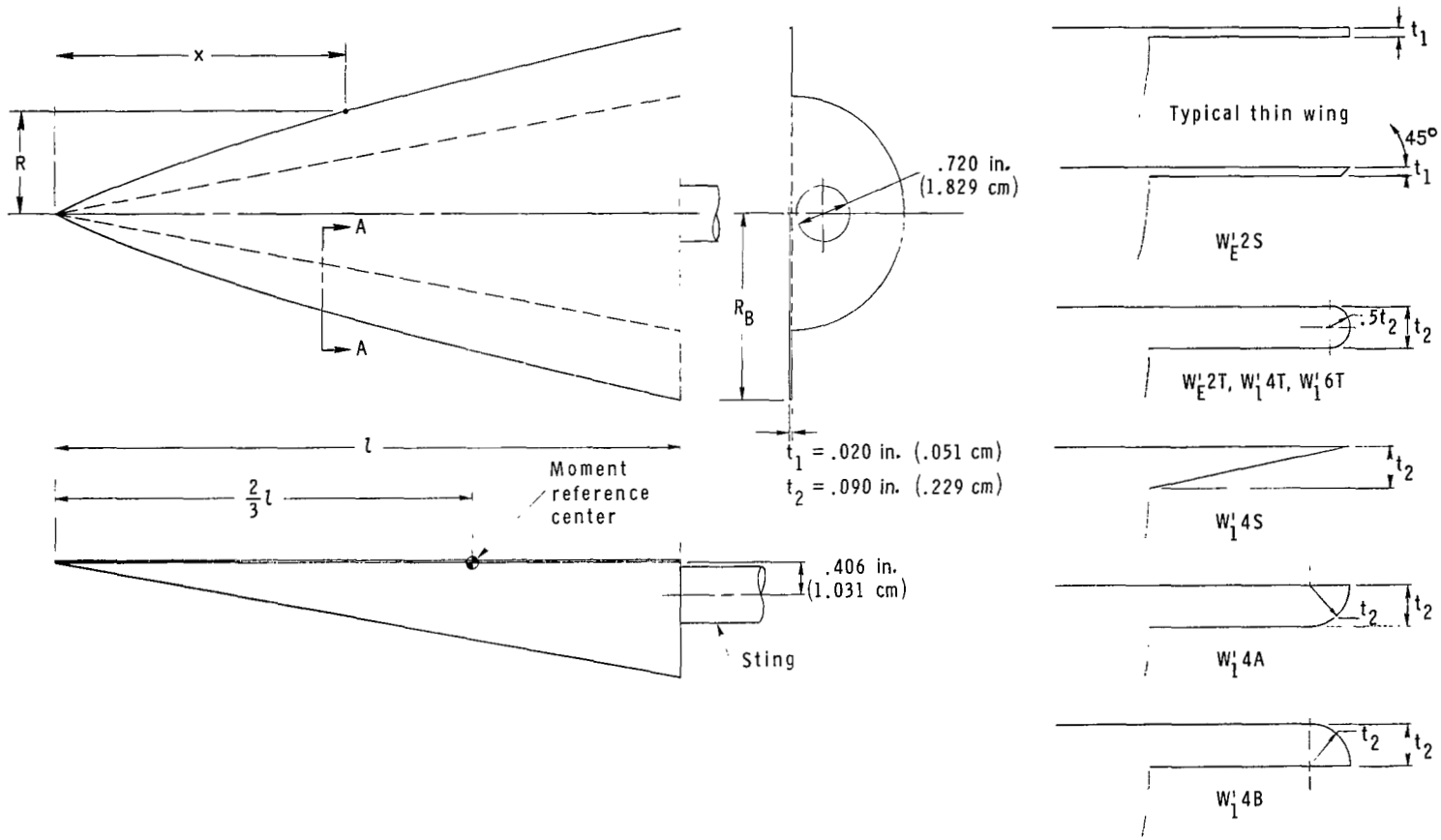

(a) Model configuration and sting location. (Table I gives dimensions and table II gives curved leading-edge planforms.)

(b) Section A-A showing leading-edge shapes. (Enlarged scale.)

Figure 1.- General model configuration and leading-edge shapes.

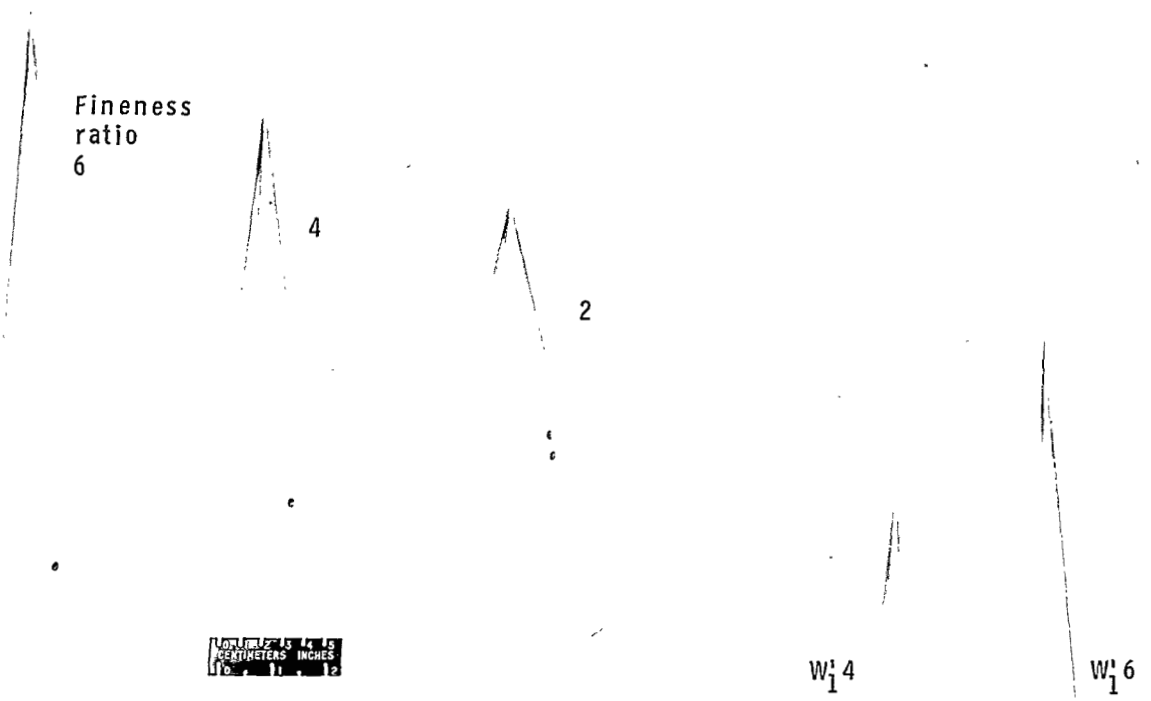

(a) Full-cone models.

(b) Three models of cone fineness ratio 4.

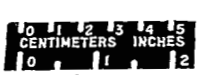

(c) Edge view of deformed wings.

Figure 2.- Several models used in present study. L-70-1627

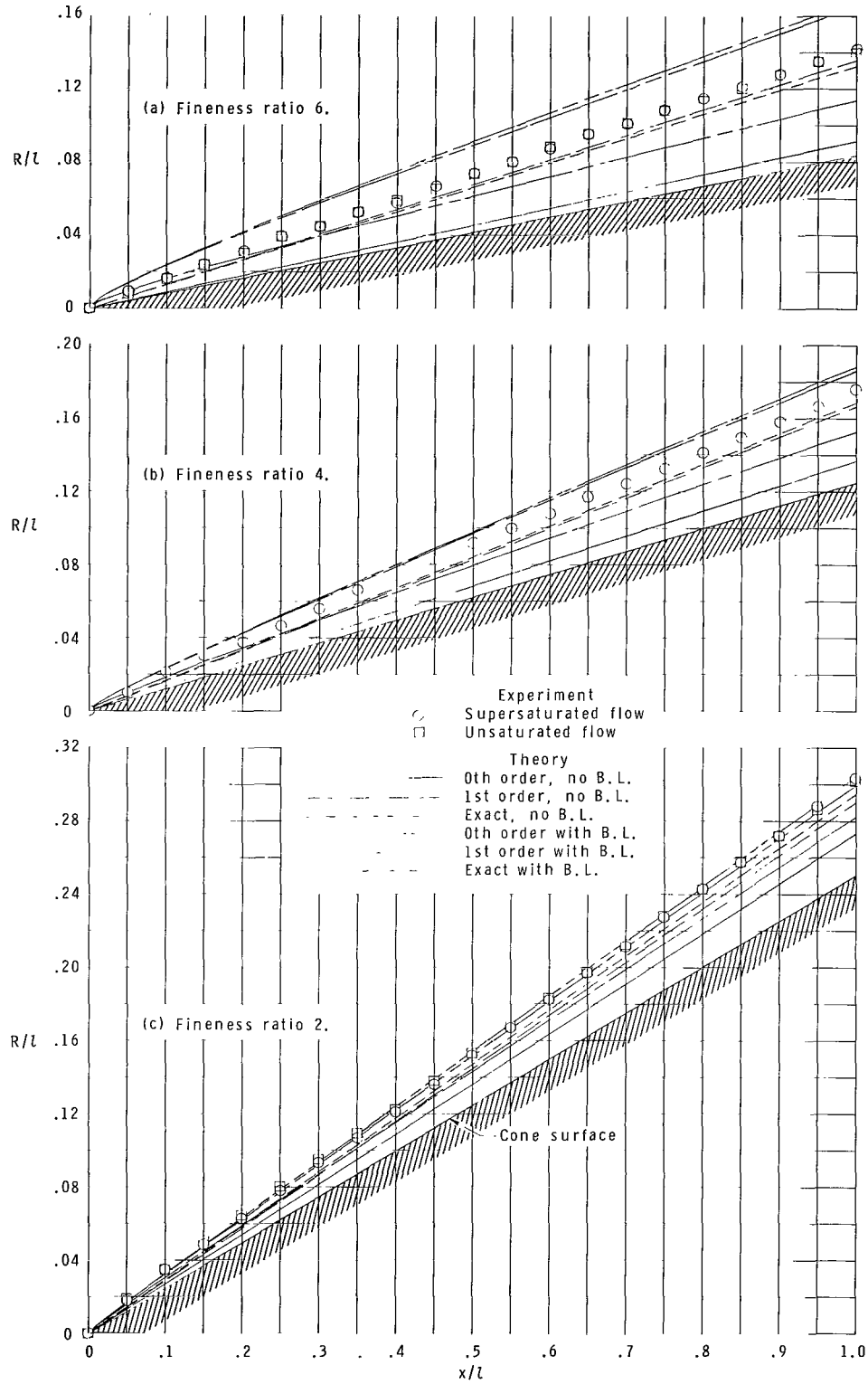

Figure 3.- Experimental and theoretical shock-wave shapes about full cones.

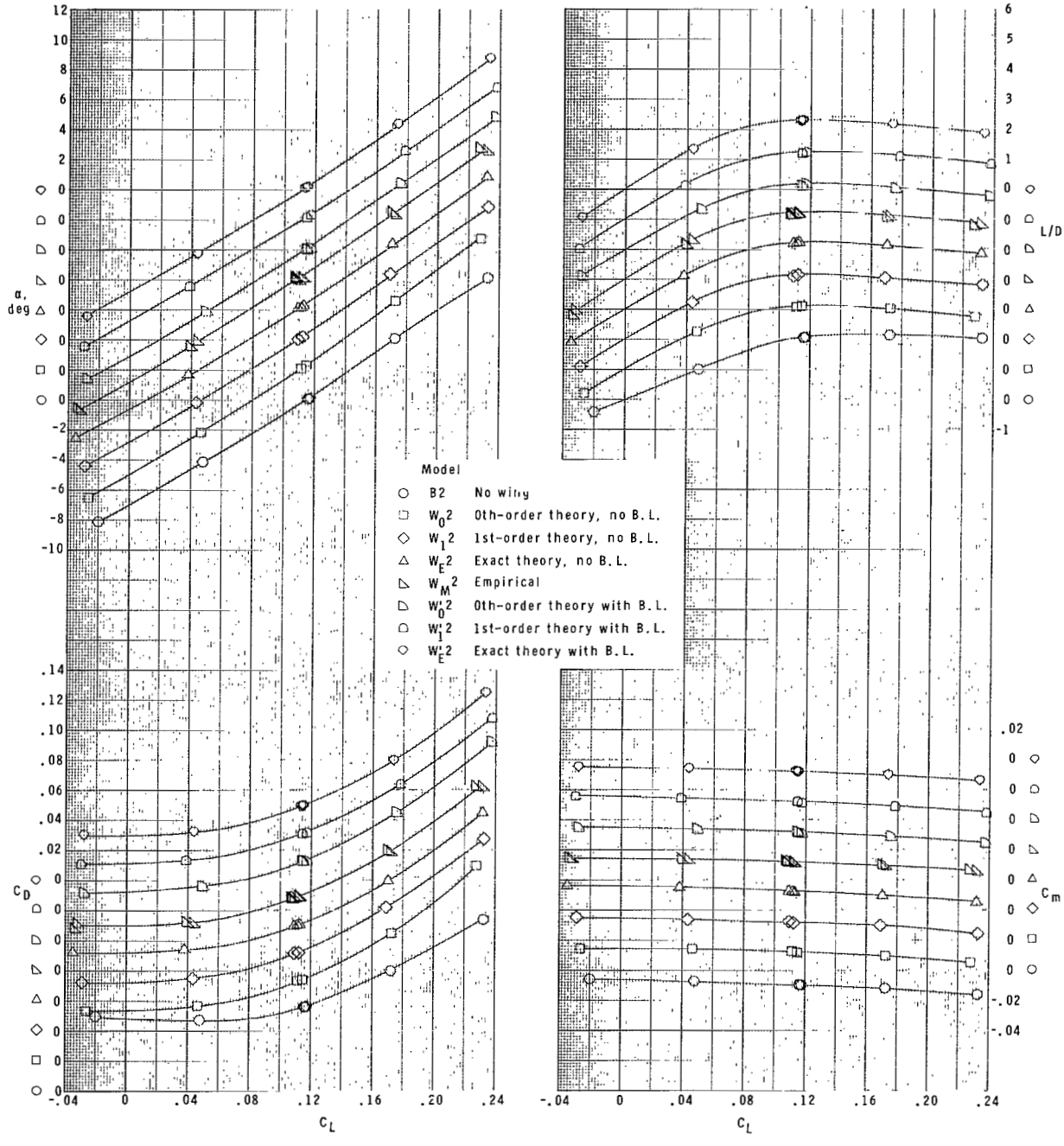

(a) Cone fineness ratio 2.

Figure 4.- Aerodynamic characteristics of several model configurations.

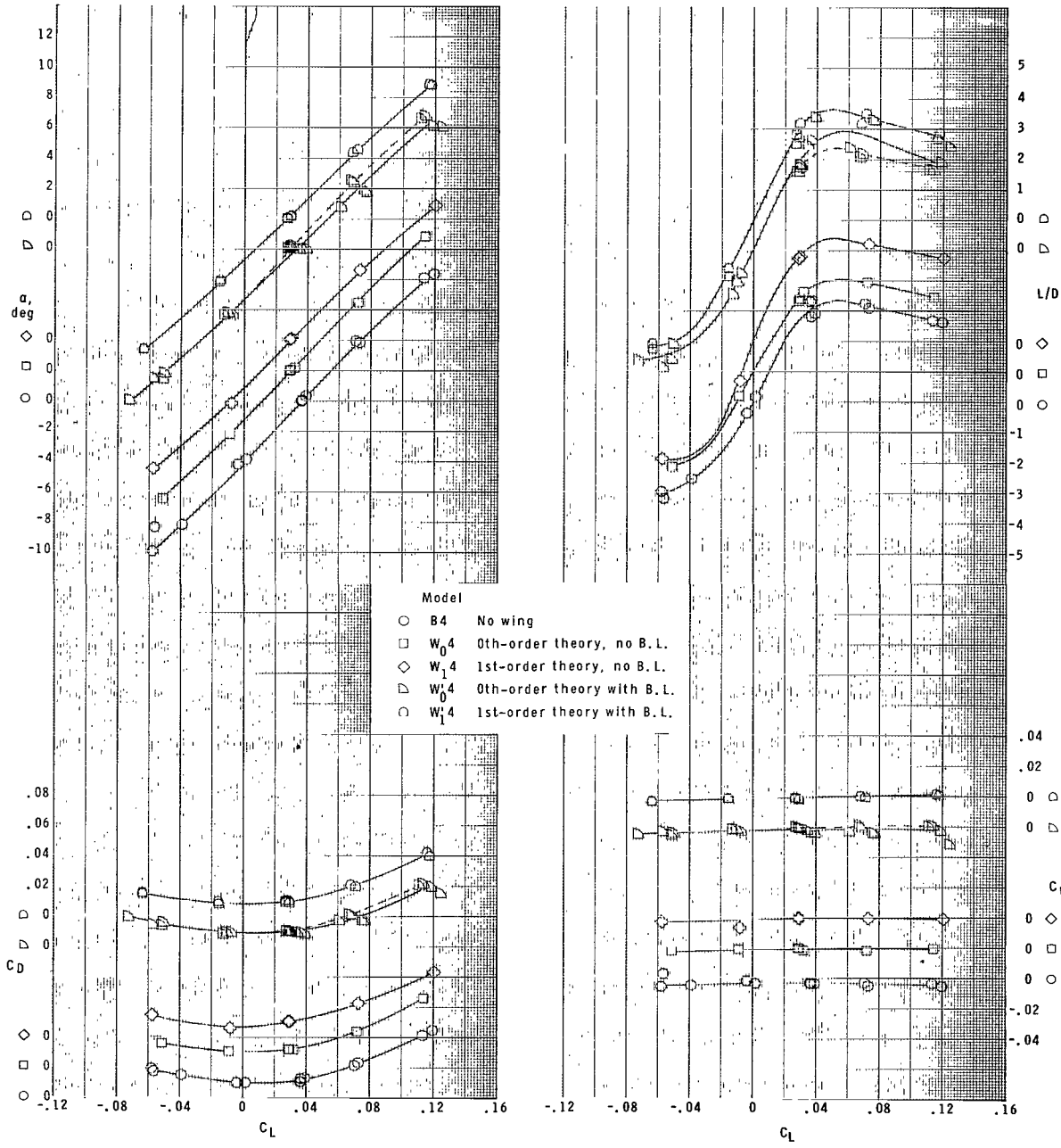

(b) Cone fineness ratio 4.

Figure 4.- Continued.

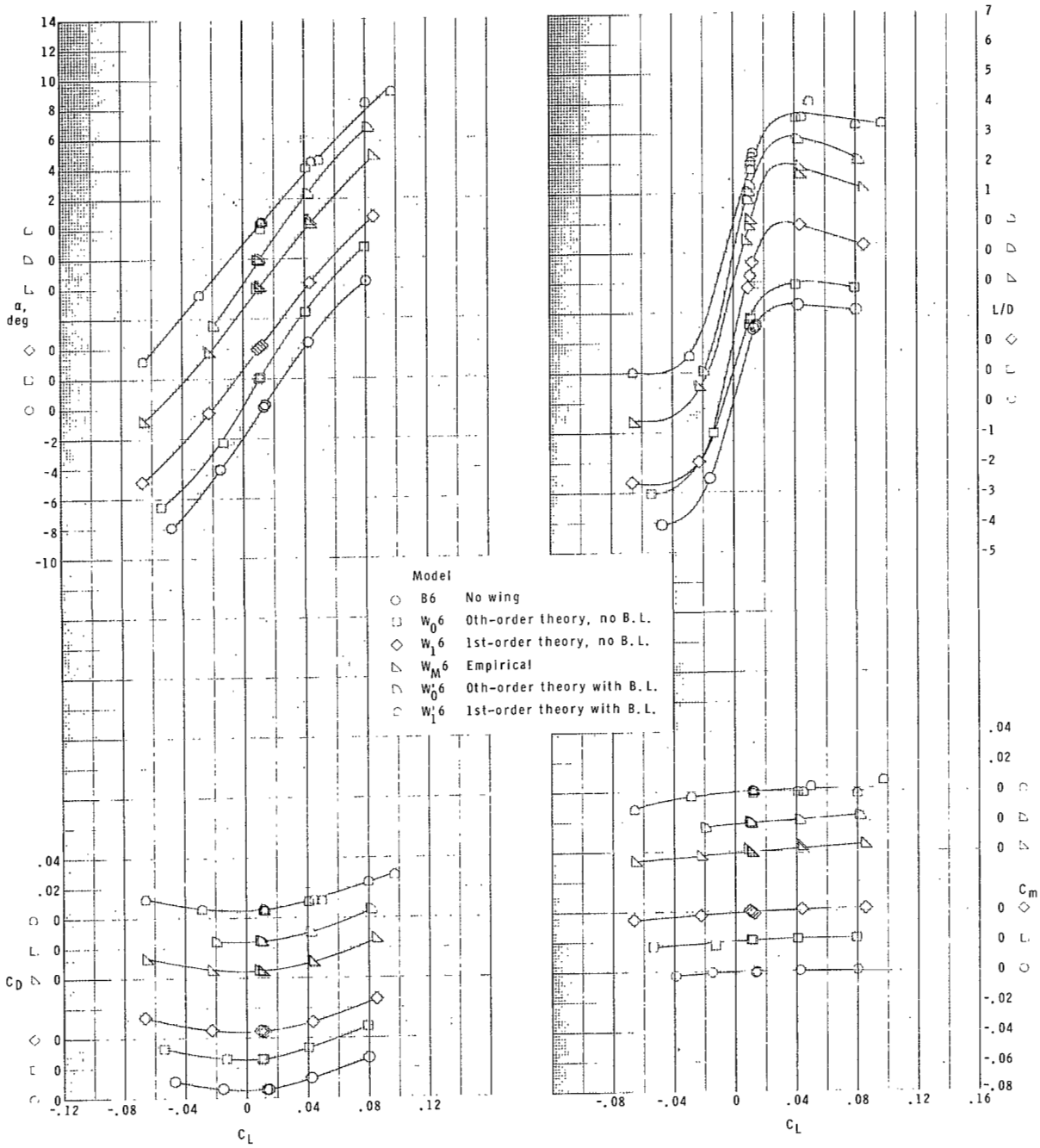

(c) Cone fineness ratio 6.

Figure 4.- Concluded.

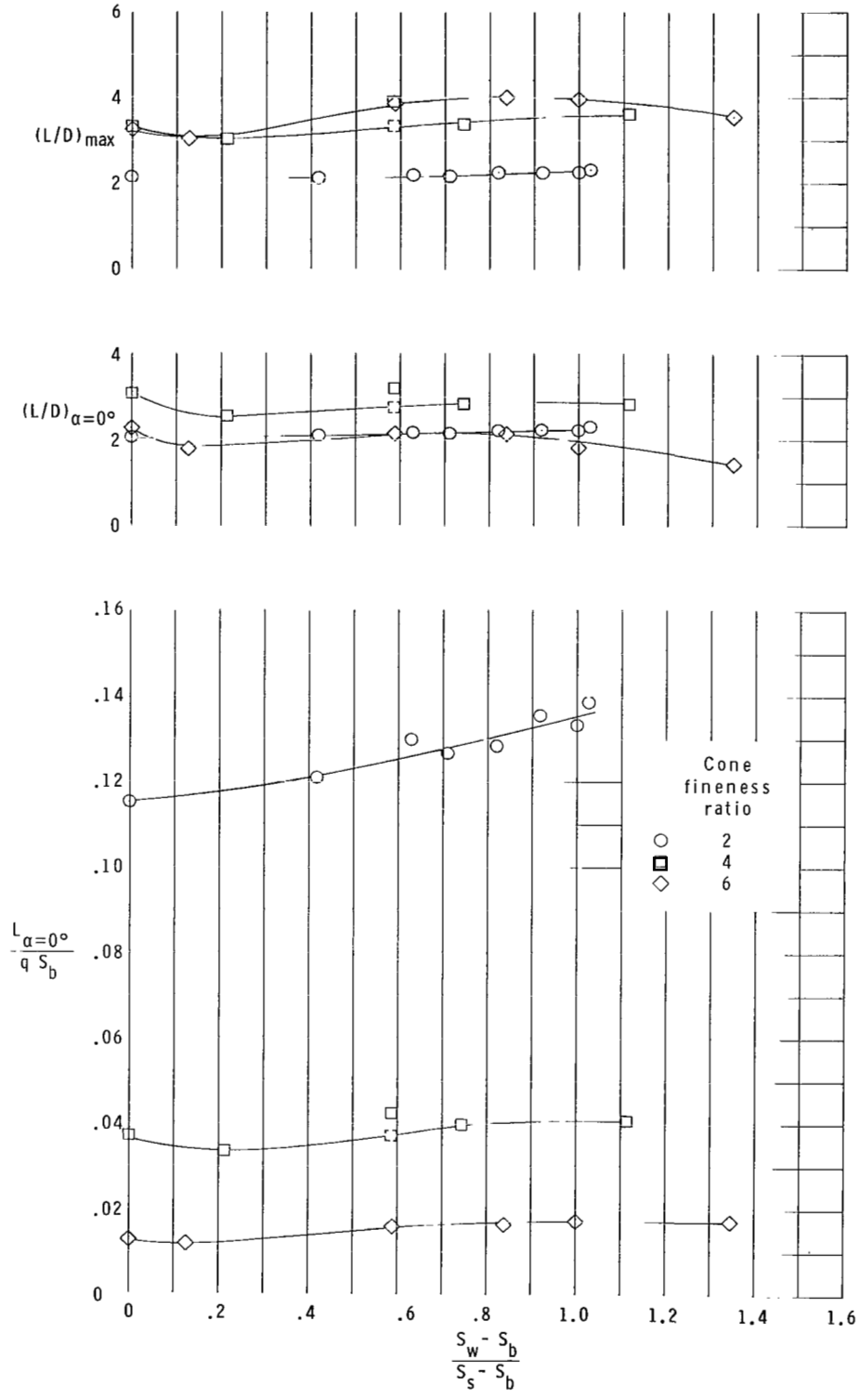

Figure 5.- Summary of wing-planform-area effects.

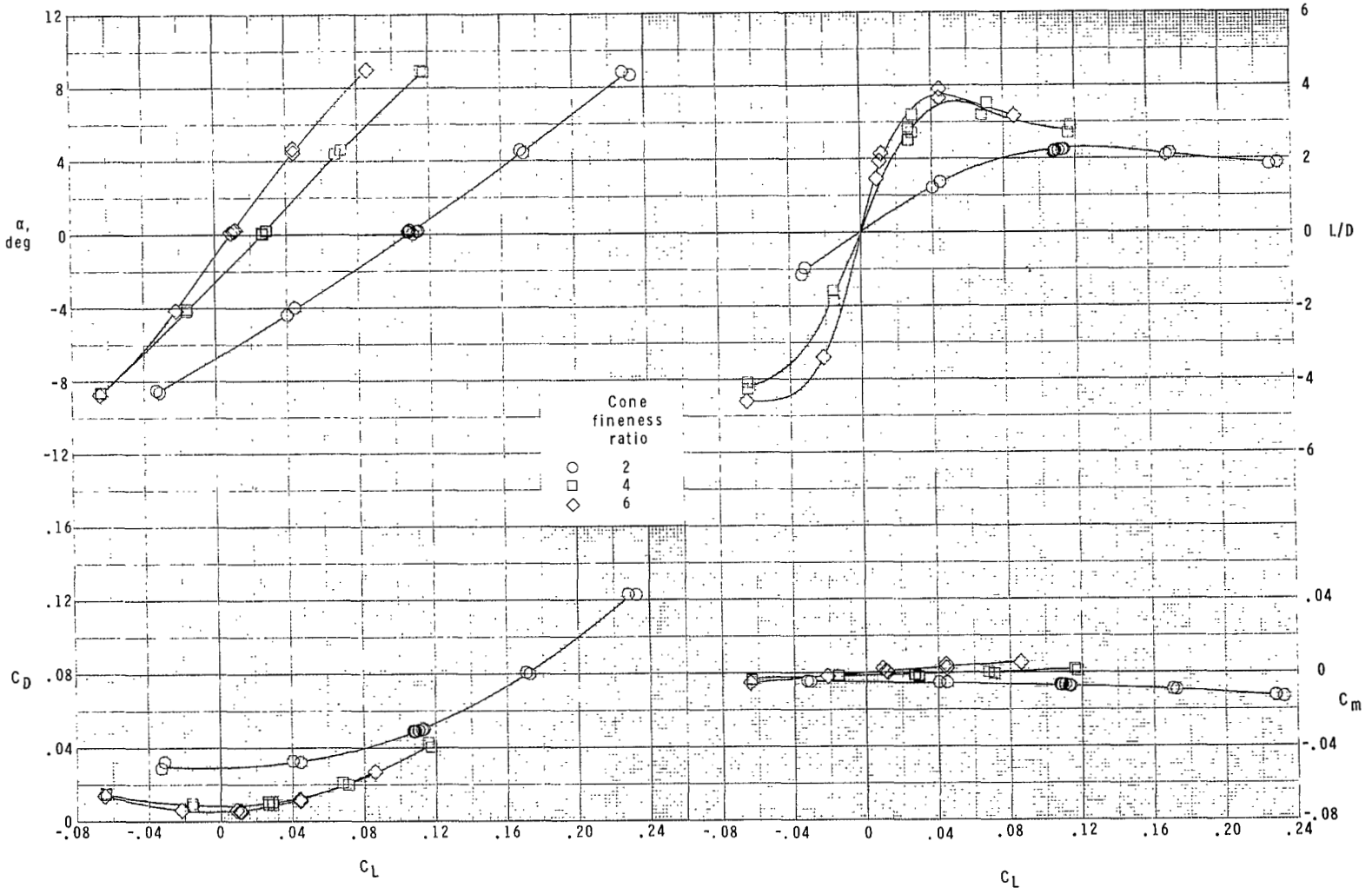

(a) Empirical planform wings.

Figure 6.- Effect of fineness ratio on aerodynamic characteristics.

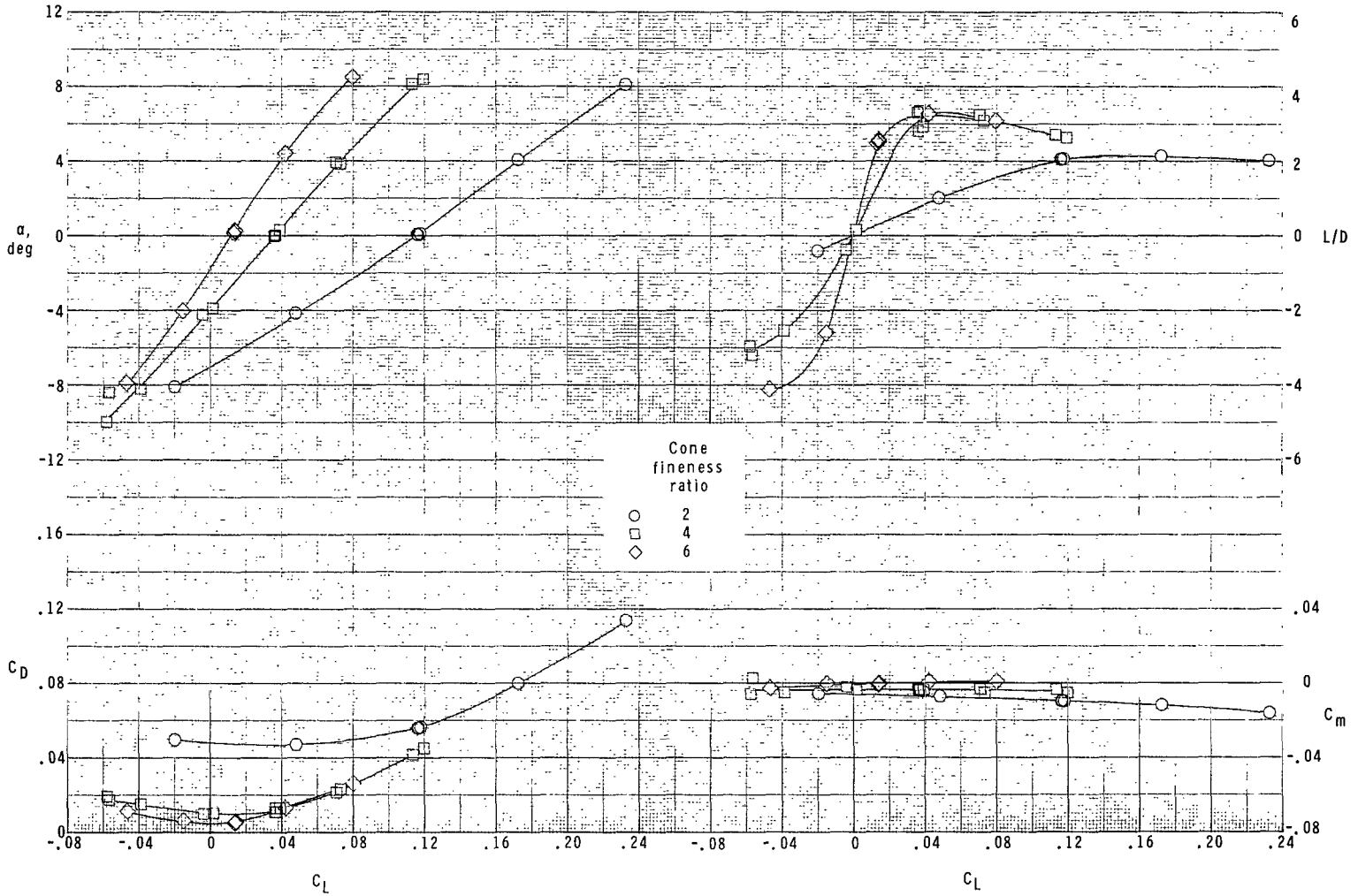

(b) Half-cone bodies alone (no wing).

Figure 6.- Concluded.

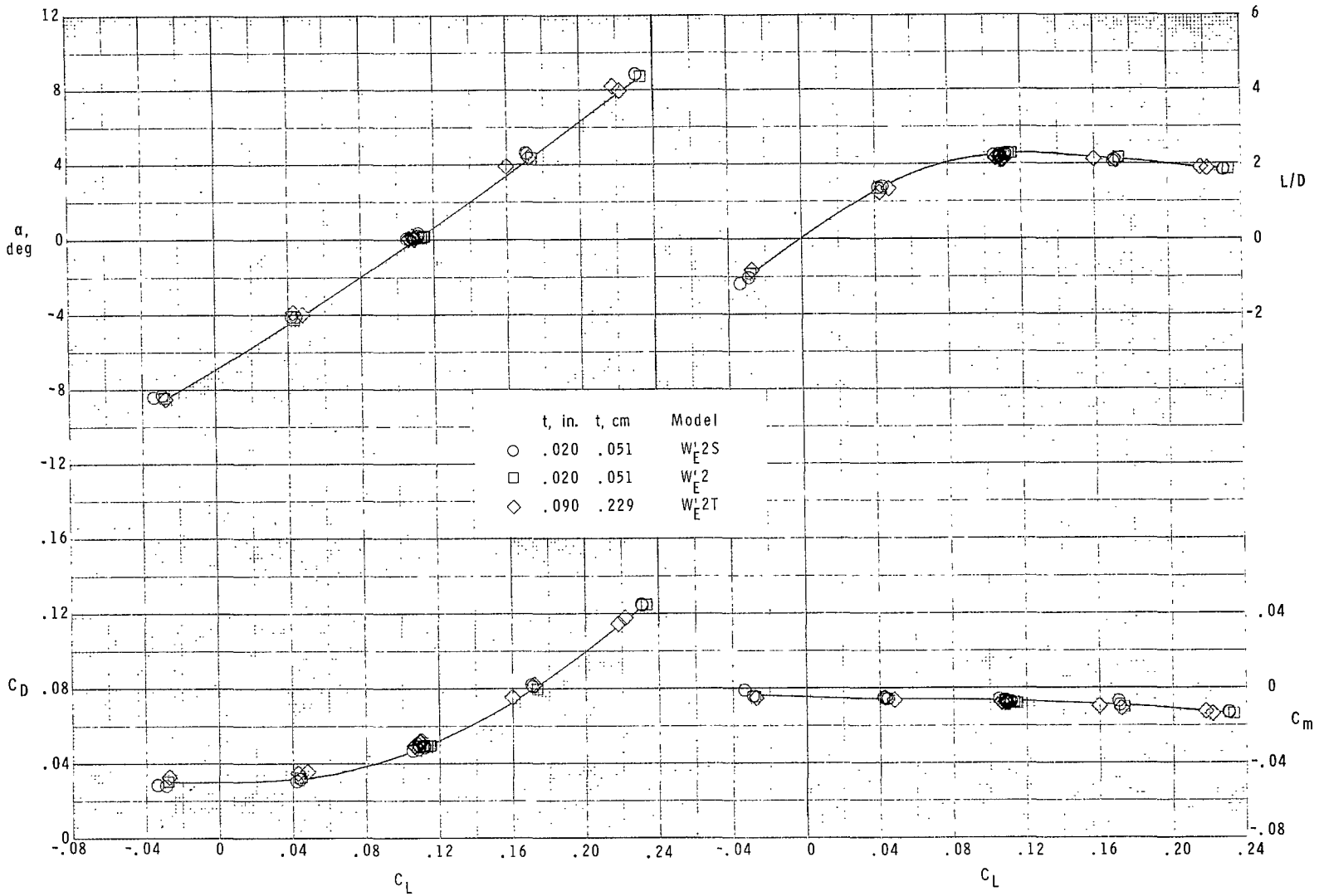

(a) Cone fineness ratio 2.

Figure 7.- Effect of wing leading-edge thickness and shape on aerodynamic characteristics.

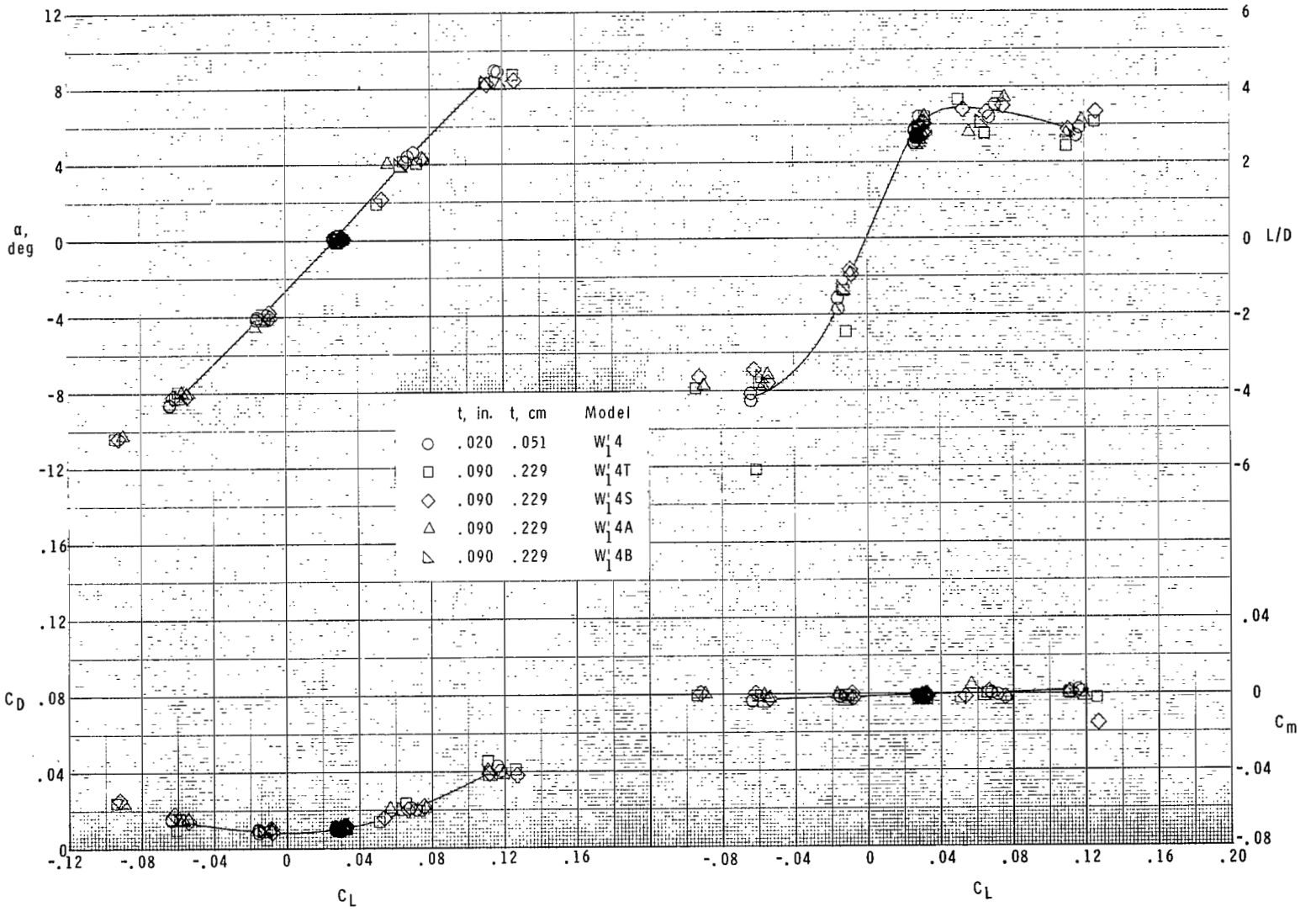

(b) Cone fineness ratio 4.

Figure 7.- Continued.

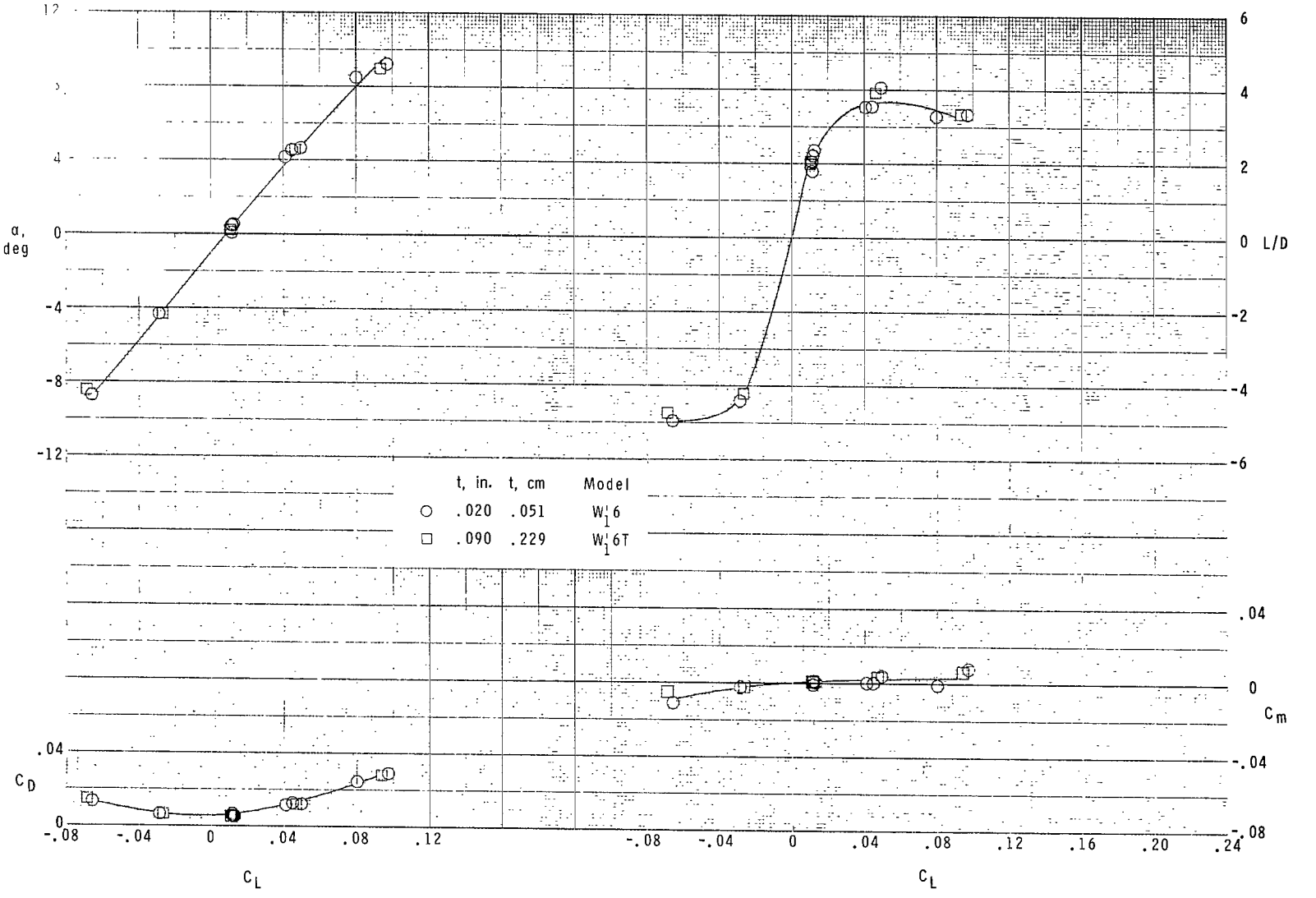

(c) Cone fineness ratio 6.

Figure 7.- Concluded.

NATIONAL AERONAUTICS AND SPACE ADMINISTRATION
WASHINGTON, D.C. 20546

OFFICIAL BUSINESS

FIRST CLASS MAIL

POSTAGE AND FEES PAID
NATIONAL AERONAUTICS AN
SPACE ADMINISTRATION

"The aeronautical and space activities of the United States shall be conducted so as to contribute . . . to the expansion of human knowledge of phenomena in the atmosphere and space. The Administration shall provide for the widest practicable and appropriate dissemination of information concerning its activities and the results thereof."

—NATIONAL AERONAUTICS AND SPACE ACT OF 1958

NASA SCIENTIFIC AND TECHNICAL PUBLICATIONS

TECHNICAL REPORTS: Scientific and technical information considered important, complete, and a lasting contribution to existing knowledge.

TECHNICAL NOTES: Information less broad in scope but nevertheless of importance as a contribution to existing knowledge.

TECHNICAL MEMORANDUMS: Information receiving limited distribution because of preliminary data, security classification, or other reasons.

CONTRACTOR REPORTS: Scientific and technical information generated under a NASA contract or grant and considered an important contribution to existing knowledge.

TECHNICAL TRANSLATIONS: Information published in a foreign language considered to merit NASA distribution in English.

SPECIAL PUBLICATIONS: Information derived from or of value to NASA activities. Publications include conference proceedings, monographs, data compilations, handbooks, sourcebooks, and special bibliographies.

TECHNOLOGY UTILIZATION PUBLICATIONS: Information on technology used by NASA that may be of particular interest in commercial and other non-aerospace applications. Publications include Tech Briefs, Technology Utilization Reports and Notes, and Technology Surveys.

Details on the availability of these publications may be obtained from:

SCIENTIFIC AND TECHNICAL INFORMATION DIVISION

NATIONAL AERONAUTICS AND SPACE ADMINISTRATION

Washington, D.C. 20546